Aalto University

Aria, Shafa; Azevedo, Rui; Burow, Rick; Cahill, Fiachra; Ducheckova, Lada; Holroyd, Alexa;
Huarcaya, Victor; Järvelä, Emilia; Koßagk, Martin; Moeckel, Chris; Rodriguez-Aramendia,
Ana; Royer, Fabien; Sypniewski, Richard; Vittori, Edoardo; Yttergren, Madeleine

GLINT

CrossMark

GLINT

Gravitational-wave laser INterferometry triangle

Shafa Aria[1] · Rui Azevedo[2] · Rick Burow[3] · Fiachra Cahill[4] ·
Lada Ducheckova[5] · Alexa Holroyd[6] · Victor Huarcaya[7] · Emilia Järvelä[8] ·
Martin Koßagk[9] · Chris Moeckel[10] (ID) · Ana Rodriguez[11] · Fabien Royer[12] ·
Richard Sypniewski[13] · Edoardo Vittori[14] · Madeleine Yttergren[15]

✉ Chris Moeckel
  mockel.chris@gmail.com

  Shafa Aria
  shafaa@fys.uio.no

  Rui Azevedo
  rplazevedo@gmail.com

  Rick Burow
  ruslan.burow@gmail.com

  Fiachra Cahill
  fiachra.cahill.2009@mumail.ie

  Lada Ducheckova
  ducheckovalada@seznam.cz

  Alexa Holroyd
  alexaholroyd@gmail.com

  Victor Huarcaya
  victor.huarcaya@u.nus.edu

  Emilia Järvelä
  emilia.jarvela@aalto.fi

  Martin Koßagk
  martin.kossagk@gmail.com

  Ana Rodriguez
  rodara.ana@gmail.com

  Fabien Royer
  fabien.royer@supaero.isae.fr

  Richard Sypniewski
  rhsypnie@gmail.com

  Edoardo Vittori
  edoardo.vittori12@ic.ac.uk

  Madeleine Yttergren
  m.yttergren@gmail.com

⚛ Springer

Abstract When the universe was roughly one billion years old, supermassive black holes (10^3-10^6 solar masses) already existed. The occurrence of supermassive black holes on such short time scales are poorly understood in terms of their physical or evolutionary processes. Our current understanding is limited by the lack of observational data due the limits of electromagnetic radiation. Gravitational waves as predicted by the theory of general relativity have provided us with the means to probe deeper into the history of the universe. During the ESA Alpach Summer School of 2015, a group of science and engineering students devised GLINT (Gravitational-wave Laser INterferometry Triangle), a space mission concept capable of measuring gravitational waves emitted by black holes that have formed at the early periods after the big bang. Morespecifically at redshifts of $15 < z < 30$ ($\sim 0.1 - 0.3 \times 10^9$ years after the big bang) in the frequency range $0.01 - 1$ Hz. GLINT design strain sensitivity of 5×10^{-24} $1/\sqrt{\text{Hz}}$ will theoretically allow the study of early black holes formations as well as merging events and collapses. The laser interferometry, the

[1]   University of Oslo, Boks 1072, Blindern, 0316, Oslo, Norway

[2]   Faculdade de Ciências da Universidade do Porto, Rua do Campo Alegre, s/n, 4169-007 Porto, Portugal

[3]   Universität Bremen, Bibliothekstraße 1, 28359 Bremen, Germany

[4]   Maynooth University, National University of Ireland, Maynooth, Ireland

[5]   Czech Technical University of Prague, Brehova 7, Praha 1, 11519 Czech Republic

[6]   University of Bristol, Senate House, Tyndall Avenue, Bristol, BS8 1TH, UK

[7]   Centre for Quantum Technologies/National University of Singapore, S15 02-05, 3 Science Drive 2, Singapore 117543 Singapore

[8]   Aalto University Metsähovi Radio Observatory, Metsähovintie 114, 02540, Kymälä, Finland

[9]   Technical University Dresden / Institute of Aerospace Engineering, Marschnerstraße 32, 01307 Dresden, Germany

[10] Delft University of Technology, Kluyverweg 1, 2629 HS Delft, Netherlands

[11] University of Vienna / Institute for Quantum Optics and Quantum Information, Boltzmanngaße 3, 1090 Vienna, Austria

[12] Institut Supérieur de l'Aéronautique et de l'Espace, Campus SUPAERO 10 Avenue Édouard Belin, 31400 Toulouse, France

[13] FOTEC Forschungs- und Technologietransfer GmbH, Viktor Kaplan-Strasse 2, 2700 Wiener Neustadt, Austria

[14] Imperial College London, London SW7 2AZ, UK

[15] Chalmers University of Technology, Chalmersplatsen 4, 412 58 Gothenburg, Sweden

technology used for measuring gravitational waves, monitors the separation of test masses in free-fall, where a change of separation indicates the passage of a gravitational wave. The test masses will be shielded from disturbing forces in a constellation of three geocentric orbiting satellites.

Keywords Gravitational waves · Supermassive black holes · Laser interferometry

1 Introduction

Our current understanding of the universe is based on the detection of electromagnetic radiation, which ranges from low-frequency radio waves to very high-energy gamma rays. Electromagnetic radiation provides a useful but limited view into our universe because it interacts strongly with matter, making it susceptible to absorption and scattering. Even though this interaction occurs more strongly with infrared radiation, the expansion of the universe causes the visible light from very far away objects to be redshifted into wavelengths that are then either scattered/absorbed by dust or that are beyond the detection range of our telescopes. One of the most distant sources we have been able to observe are bright quasars which are believed to be powered by supermassive black holes (SMBH). So far over forty quasars with redshifts of more than $z = 6$ have been discovered ([81] and references therein), each of them harboring a black hole of several billion solar masses. The existence of SMBH at this early age of the universe (roughly one billion years after the big bang), is not currently explained [31]. The number of the SMBH is too large to be produced at such a young age of the universe.

General relativity, published by Albert Einstein in 1915, describes another way to observe the universe. It predicts that accelerating massive objects emit energy as gravitational waves that propagate freely through the universe at the speed of light. Unlike electromagnetic radiation, gravitational waves do not interact with matter and thus can be considered undisturbed. Therefore, they are currently the only known method to obtain information regarding events far into the past, such as SMBH formation. With recent advances in technology [6, 8, 26, 82] this new window into the universe will open as gravitational wave astrophysics further develops our understanding of the universe.

This paper presents the results from a student exercise during ESA Alpbach Summer School in 2015. A group of 15 students were asked to design a mission concept for the astrophysical community and GLINT, a space-based laser interferometer, was designed to study several phenomena, with its main focus on the early period in the universe. The report first details the scientific objects of interest in Section 2, and then describe the type of signal to be measured in Section 3. The instrument architecture is detailed in Section 4, and the associated major technical challenges are listed in Section 5. The detailed spacecraft design is given in Section 6 and the ground infrastructure shortly mentioned in Section 7. The conclusions summarize the main points of the report in Section 8.

2 Science with GLINT

GLINT main focus is to investigate the formation and evolution of the first black holes, occurring $0.1 - 0.3$ billion years after the big bang, allowing the study of a previously unexplored period in the universe. GLINT is designed to study the frequency range between 0.01-1 Hz, over which its strain sensitivity is as low as 5 $\times$ 10^{-24} $1/\sqrt{Hz}$. This design sensitivity is chosen to provide information on black holes themselves, inspiraling of mass into black holes, as well as the mannerisms of binary systems, for example, which objects compose binary systems and how different combinations of binary systems behave.

The subsequent sections elaborate on the theoretical background, the method of detection of gravitation waves and deduction of information, as well as the spacecraft design and the mission profile.

Gravitational waves When a massive object undergoes an asymmetric collapse, its quadrupole moment changes and it creates ripples in spacetime, which propagate as waves [43]. These waves are called gravitational waves and are characterized by an observer by their frequency, strain, and polarization. Strain, $h \equiv \frac{\Delta L}{L}$, is defined as the dimensionless fractional stretching and squeezing of spacetime as a gravitational wave passes through.

Indirect proof of gravitational waves comes from the observations of the binary pulsar PSR 1913+16, found in 1974 by Hulse and Taylor [41]. The orbital decay of the binary system due to the energy loss via gravitational wave emission is in excellent agreement with the predictions from General Relativity. in 2016, direct proof has been obtained by the Laser Interferometer Gravitational-Wave Observatory (LIGO), which detected gravitational waves produced by a binary black hole merger [48].

The first black holes Stellar-mass black holes are formed when massive stars reach the end of their life. The masses of these stars are in the range of a few solar masses to tens of solar masses. If the first black holes in the universe were stellar-mass black holes they would have needed to constantly accrete at a maximum rate after their formation to become the SMBH we observe at redshifts $z > 6$. This scenario is highly improbable since several different feedback mechanisms limit the black hole growth via accretion (such as [54, 66]). Current theories predict that the formation of the first black holes might have been very different from what we see now in the local universe. Plausible scenarios for the early black hole formation are the collapse of supermassive stars (SMS), direct collapse black holes (DCBH), and the collapse of very massive objects (VMO).

SMS are some of the very first stars formed, called Population III stars. Due to environmental conditions in the early age of the universe, they were able to reach masses of 260-800 $M_\odot$ and they consisted solely of hydrogen. These massive stars were very short-lived and formed black holes with mass $M = 10^2 - 10^3 M_\odot$ via core collapse [35]. According to numerical simulations [35] the SMSs collapsing into black holes at redshifts ~20-30 would be observable at frequency range 0.4-1 Hz with GLINT. Their expected strain is $\sim 20 \times 10^{-24}$, which is well above the

sensitivity limit of GLINT as seen in Figs. 1 and 5. An optimistic estimate for their production rate is 10^7 per year.

DCBH are formed when a very atomic hydrogen gas cloud collapses directly into a black hole due to gravitational attraction. After the first DCBH formed they triggered further direct collapses into black holes [84], resulting in a large amount of intermediate mass black holes (IMBH). These IMBH have masses of $10^4 - 10^6$ $M_\odot$ [84] and are believed to either be embedded in galaxies or to have merged into a SMBH. Their expected production rate is 10^4 per year and the strain is of order of 10^{-23} at the frequency range 0.01-0.1 Hz [61].

VMO [70] usually refers to either SMS, which were already discussed, or clusters consisting of stars and gas, usually with masses of 10^2-10^5 $M_\odot$. The clusters began their collapse by merging a few stars and some gas, which leads to a runaway process where the mass continues to fall together, eventually resulting in a IMBH. VMOs would be observable from 0.01 to 0.2 Hz with a strain of $\sim 10^{-23}$ and a production rate of 4000 per year [70].

Evolution of black holes When a black hole has been formed it continues to grow through different processes: accretion, inspirals, and mergers [6]. Accreting black holes gather mass rather slowly and are limited by radiation pressure and feedback processes. Black holes can also grow through inspiraling of a stellar-mass black hole, neutron star, and white dwarf. The most efficient way to increase the mass is the coalescence of two black holes. The first black holes grew periodically through one of these processes or a combination of them to evolve into a SMBH.

Additional observable events Besides SMS, DCBH and VMO, there are additional objects that GLINT could observe in its operating frequency range. Among these are neutron star binaries and extreme mass inspiraling into a black hole [6, 16, 58]. These objects are important for testing the General Relativity theory and also to understand the specifics of how such systems behave.

Cosmology and the theory of gravitation Some of the most important questions in cosmology are related to the composition of the universe in terms of matter and dark energy densities. These quantities describe how the current universe behaves and evolves on a large scale.

A gravitational wave detector, such as GLINT, is able to determine the direction and luminosity distance, D_L, of inspirals and binaries. If these gravitational wave sources emit radiation (e.g. X-ray emission during inspirals), or if they are located within host systems that emit radiation, we can use electromagnetic wave observations from future observatories that will succeed ESA's Athena X-ray telescope or NASA's James Webb Space Telescope (JWST) to calculate the redshift of these systems. From the standard Lambda - Cold Dark Matter Model cosmological model, we know that the luminosity distance, D_L, is related to the redshift, z by

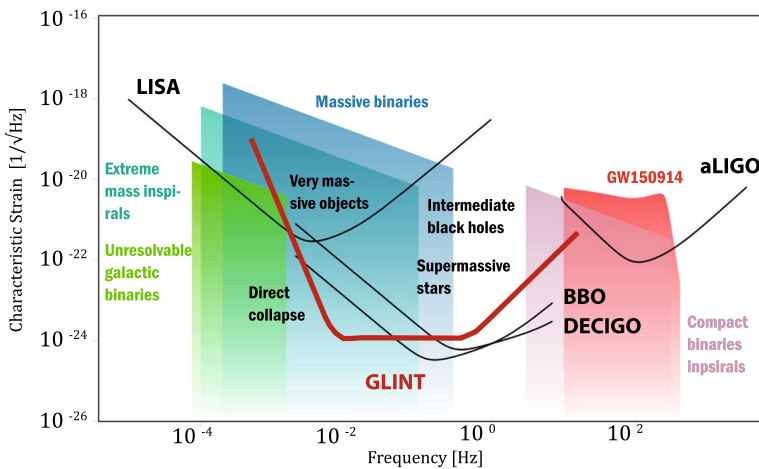$$D_L(z) = \frac{c}{H_0}(1+z)\int\limits_0^z \frac{dz'}{\sqrt{\Omega_m(1+z')^3 + \Omega_\Lambda}}, \tag{1}$$

Fig. 1 Illustration depicting the strain ($1/\sqrt{Hz}$) of different sources. This is the gravitational wave spectrum with current and planned detector sensitivities superimposed. Original data are obtained from [58] and are visualized by http://rhcole.com/apps/GWplotter

where H_0 is the Hubble constant as of today, Ω_m is the matter density, and Ω_Λ is the dark energy density. Knowing the luminosity distance and the redshift for a certain event then allows us to establish constraints on the ratio between the matter and dark energy densities.

The measurement of certain events will also allow for a comparison against theoretical models including ones provided by other theories of gravitation, e.g. $f(R)$ and non-minimal coupling [5, 80, 83]. While these theories are already highly constrained in the weak-field regimes, one must also test gravity in the strong-filed regimes. However, since the usual Parametrized Post-Newtonian formalism is not well suited for these tests, comparisons with theoretical models may have to resort to numerical simulations, similarly to the present case with General Relativity.

GLINT can also complement other past, ongoing and planned experiments that map the dark matter distribution such as Planck [3], Euclid [47], and the Large Synoptic Survey Telescope [79]. While unable to locate GW source with pinpoint accuracy, the detection of the same signal multiple times due to strong lensing could provide constraints on H_0 and dark energy, as well as test the propagation velocity of gravity and provide insight into the formation of large scale structures in the Universe [73].

Other missions Whereas we can not directly observe black holes, we can study their effect on matter. Black holes that are actively accreting matter, for example, in active galactic nuclei and micro quasars, produce observable electromagnetic radiation consequent to the accretion processes [19]. Black hole related emission can be observed over the whole electromagnetic spectrum, from radio to gamma-rays, and includes a variety of long-lasting phenomena, for example, the relativistic plasma jets, the accretion disk and the hot corona [42, 44, 57, 77], as well as transient phenomena, such as the tidal disruption events [4]. The redshifts studied here cannot be reached

with any currently known method, due to the limitations of electromagnetic radiation detection. Other gravitational wave antennas, such as LIGO [1], VIRGO [2], and GEO600 [30] are already in operation on Earth, but their sensitivities at low frequencies ($< 10\,Hz$) are limited by the arm lengths, seismic noise, and by interference from nearby moving masses.

At present time there are a number of space-based missions proposed. Two noteworthy projects are the Japanese DECi-hertz Interferometer Gravitational wave Observatory (DECIGO) concept and the European Laser Interferometer Space Antenna (LISA) concept. The DECIGO proposal is still in a very early conceptual stage due to the technical challenges related to the envisioned interferometry method. It plans on observing gravitational waves to study cosmology in a frequency range of $0.1 - 10\,Hz$ [82], though its mission status is currently uncertain. LISA is an ESA study planned to observe gravitational waves in the frequency range of $0.1\,\text{mHz} - 1\,\text{Hz}$, the best sensitivity of $10^{-20}\,\text{Hz}^{-1/2}$ encompasses the gravitational wave frequency range of $0.3 - 5\,\text{mHz}$ [24].

Several projects regarding LISA technology and mission design are ongoing in the United States and Europe, e.g. fundamental research with LISA [7], and the technology advancement with LISA Pathfinder [9]. The LISA Pathfinder was launched in late 2015 with the aim to prove key technologies used for space-based laser interferometry, the first in-flight results arrived in June 2016, Armano et al. [11]. Furthermore, LISA is planned for ESA's third large mission launch slot in the Cosmic Vision program, with a target launch date in 2034. Its primary objective is to detect and measure gravitational waves produced in the earliest stages of the Big Bang, from compact binary systems and mergers of SMBH, where the total mass of the merging systems is in the range 10^4 - 10^7 M$\odot$ [37]. Figure 1 represents the sensitivity and the frequency ranges for the different ongoing and proposed missions, including GLINT.

2.1 Summary of GLINT science

The unprecedented sensitivity of GLINT in the frequency range of $0.1 - 1\,\text{Hz}$ opens up a window into the effect of gravity on the very first extraordinary massive objects, the progenitors to the first black holes. Therefore, GLINT will be able to answer:

- When did the first black holes of several solar masses appear?
- How did they form?
- At what rate did they form?
- What are their properties (mass, spin and charge)?
- How did they evolve (mergers, inspirals, accretion)?

In addition to this, GLINT also has the ability to provide a greater understanding of binary systems, and thus to answer these questions:

- How do binary star systems of different masses behave?
- What objects (stars, black holes, etc) compose a binary systems?

The expected rates of the events GLINT will study are listed in Table 1.

Science with data from complementary experiments GLINT data can be combined with data from other experiments in the electromagnetic spectrum to constrain cosmological models, i.e. address the following:

- How did the universe evolve and what are dark matter and dark energy densities?

While this objective is not unique to GLINT, it could provide additional information in conjunction with current measurements from observatories such as Planck [65]. It also demonstrates the viability of concurrent and multi-frequency observation in the electromagnetic and gravitational spectra, which remains untested as of now, largely due to the infancy of gravitational wave astronomy.

2.2 Scientific objectives

For a redshift of $z = 6$, the following objects produce a signal detectable by the design sensitivity (see also Table 1):

- The DCBH in the range of 10^4-10^6 solar masses.
- The collapse of VMO in the range of 10^2-10^5 solar masses.
- The collapse of SMS in the range of 260-800 solar masses.
- The merging event of two black holes in the range of 10^2-10^5 solar masses.
- The inspiraling of massive objects in the range of 10^2-10^3 solar masses.

Further simulations are required to obtain a more complete overview, including the relationship between the observatory orientation and the propagation plane of the gravitational waves. These studies must also focus on studying the intereference effects of several concurrent sources.

3 Science measurement

To establish an extensive understanding of black hole formation and evolution we require comprehensive data from different black hole progenitor populations spanning the redshifts $15 < z < 30$, as well as mergers of IMBH and inspirals into black holes.

The theory behind the gravitational waves has been extensively studied, and lately theories have been put to use in numerical calculations and sophisticated simulations, providing us detailed estimates, for example, for the waveforms different gravitational phenomena produce, and their expected properties, including, e.g., the strain, the frequency range and the production rate. These properties for SMS, VMO and DCBH sources are displayed in Table 1 [35, 61, 70].

To acquire the desired knowledge, GLINT must therefore measure the frequency and the strain of the gravitational wave. The polarization measurement possible with the three spacecraft design, allows for estimating the full orientation of the wave, and not only its projection on the inter-spacecraft axis. Besides providing the full amplitude of the wave, the polarization also has information about the orbital frequency of binaries around their center of mass. The signal-to-noise of the measurement is dependent on the event type, the mass of the bodies and

Table 1 Parameters of interest for the wave detection

Events	SMS	VMO	DCBH
Required sensitivity (1/$\sqrt{\text{Hz}}$)	5×10^{-24}	10^{-23}	10^{-23}
Frequency (Hz)	0.4-1	0.01-0.2	0.01-0.1
Collapse duration (s)	5-60	10-100	10-100
Production rate/year	10^7	4000	10^4

its distance from the observatory [33]. The system is designed to have a similar signal-to-noise margin as LISA of about two orders of magnitude [20], with possible advancement using match filtering techniques [34].

Due to the short event duration and the expected high event rate (see Table 1), GLINT requires only one year of measurements to be able to collect enough data to fulfil its scientific objectives. Taking into account commissioning, safe modes and additional statistics for the science measurements, a mission duration of 3 years has been designed. The approximate positions of our target sources in a strain vs. frequency plot are shown in Fig. 1. At the frequency range GLINT is using, 0.01-1 Hz, there are no significant sources of "gravitational wave noise", for example, the stochastic background is at much lower frequencies, and both, unresolvable and resolvable galactic binaries are outside of our range. Type Ia supernovae emit around 1 Hz and might be detectable with GLINT, but supernovae Ia are rather rare (about one in a century in a "normal" galaxy, such as Milky Way) and they would be detectable only to ∼1.3 Mpc [72] and thus their contribution is negligible. Lastly, the interference of multipe sources is a concern for the signal recovery. Currently, we can only estimate the number of events (see Table 1) and further information, as will be collected by GLINT, would allow to estimate interference noise and probabilties.

3.1 Models of formation and evolution of black holes

To describe the gravitational wave emitted by the acceleration of a massive object a theoretical waveform can be constructed. These waveforms are distinct for each type of event. In Fig. 2, a theoretical model of the waveform of a direct collapse black hole is depicted and in Fig. 3 an illustration of the waveform of a black hole binary merger is illustrated. The waveform of an inspiraling event is similar to the waveform of a merger, since both systems spiral before they merge, but the merger includes a ring down(a damping of the wave) after coalescence. Note, that depending on the mass of the black holes, GLINT will not be sensitive to black hole mergers as measured by LIGO-VIRGO [48], as they cover a different frequency regime (see Fig. 1). GLINT could measure such events when both objects are still in the orbital decay phase, and emit sufficient gravitational energy.

As the figures illustrate, the different events of black holes can be distinguished. There are extensive catalogues with waveforms [29, 60, 75], which can be used for analyzing and describing the particular event depending on waveform observed [64, 68]. It is important to note, however, that these are just theoretical predictions based
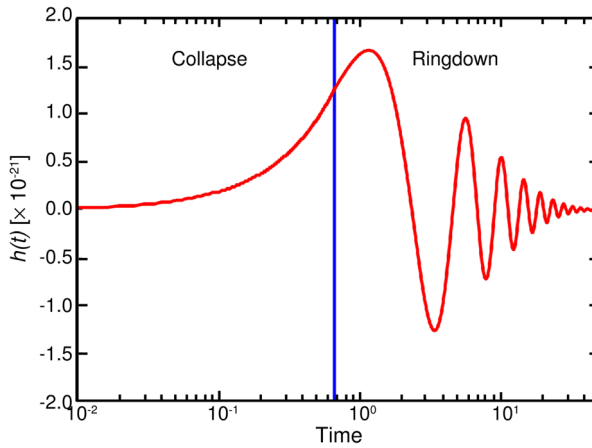
Fig. 2 A theoretical model of the waveform of the gravitational wave emitted from a cloud of gas collapsing directly into a black hole (direct collapse black hole) at redshift of z=15. The mass of the cloud is 10^5 solar masses and the mean mass density is $\rho=10^7$ g cm^{-3}. Figure from Pacucci et al. [61]

on general relativity and for very specific cases, and that it is hard to estimate the waveform and strain for some cases due to the low numbers of events in our local universe.

3.2 How to measure gravitational waves

Due to the nature of the gravitational waves, a possible way to detect them is by measuring the distance changes between free falling bodies, where all disturbing acceleration apart from gravity has been removed or have been modeled more accurately than the signal.
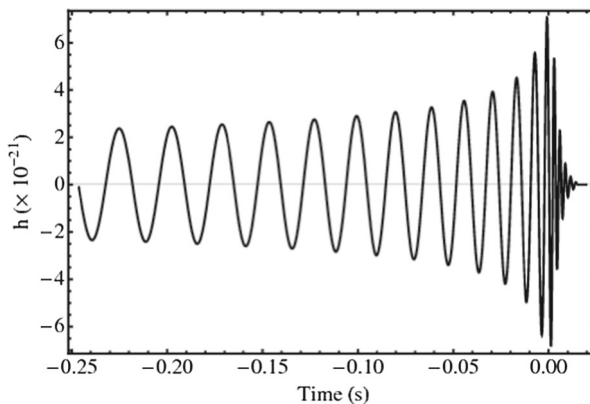

Fig. 3 The gravitational-wave strain from an optimally-oriented, i.e. so that we would observe the maximal possible amplitude, 60 solar mass non-spinning black-hole binary located 100 Mpc away from the detector. The waveform covers about six orbits, or twelve GW cycles, before merger [38]

This has associated challenges: (i) achieve very low acceleration noise due to non-gravitational forces and (ii) measure the relative distance changes of the test masses very accurately. In GLINT this is done using laser heterodyne interferometry between inertial masses provided by a drag-free control on the satellites, as explained further in the following paragraphs.

Currently, the most popular technique for measuring gravitational waves is laser interferometry, which measures the change in distance between two objects caused by the passage of a gravitational wave. There are many types of interferometers, but the two main types we looked into were the Michelson interferometry and the Fabry-Pérot interferometry.

Besides these there are other proposed ideas: atomic clocks [52], which measures the differential time dilation experienced by clocks located at different phases of a passing GW; atomic interferometry, which measures phase different between atomic waves; and Bose-Einstein Condensates [67] that measures the change in phonon excitation generated by gravitational waves passing through. However, these proposals are purely theoretical without an experimental proof yet realized.

Another method that we briefly mentioned is the use of pulsar timing arrays. This method involves the careful measurement of the arrival time of pulsar emissions to try and detect gravitational waves passing through the pulsar and/or Earth. Currently the three global projects of this type form the International Pulsar Timing array [40]. A more thorough review of this method can be found in [15, 39, 49, 53, 55].

4 Instrumentation

A trade-off of various concepts was performed that could address the scientific gap. The strongest case was made for a virtual Michelson interferometer that measures changes in the distance between gravitational reference points; in our case these points are freely falling test masses that form the end mirrors of the interferometer arms. The movements of theses masses are monitored via a free space laser link which is established between the spacecraft.

The mission concept converged to a configuration of three spacecraft in geocentric orbit and a design arm length of 100,000 km as depicted in Fig. 6. The design was driven by the requirement to obtain a sensitivity of $5 \times 10 - 24 \ 1/\sqrt{Hz}$ in the frequency range 0.01 - 1 Hz, which allows for addressing the scientific questions highlighted above.

Achieving this sensitivity level is paramount, and the spacecraft parameters and instruments specifications are designed to assure this noise level. An overview of the various error sources is given in Fig. 5, which are detailed in this section. The current iteration of the concept, therefore, highlights the technical aspects required to provide measurements in this frequency range.

Heterodyne interferometry concept GLINT will use heterodyne laser interferometry to measure the change in distance as proposed for the LISA mission [26]. This technique provides the means to measure the phase between laser beams separated

by a frequency in the MHz range. The two beams with different frequencies interfere when combined using a photo detector. The signal from the photo detector is a sine wave tied to the frequency difference. The phase changes of the signal are measured with a phase meter and indicate the relative phase between the beams which is directly proportional to the changes in distance: $\delta\phi = \frac{2\pi}{\lambda}\delta x$. This requires very sensitive measurements on the order of magnitude of $\delta\phi = 10^{-9} \text{rad}/\sqrt{\text{Hz}}$ which is assisted by the short wavelength of the laser, in our case 532 nm. A laser locking scheme in combination with a frequency plan are implemented, to keep the beat notes at a different frequency within an appropriate range. GLINT requires bandwidths of less than 20 MHz in the photodiodes and the phase meter, where the architecture is based on LISA [26]. The bandwidth requirement is derived from the relative motion of the satellites in their orbit, for LISA a 20 MHZ Doppler shift is expected compared to 3 MHz of GLINT. The distance measurements between the free falling test masses (one for each laser link) is split between the spacecrafts (SC):

- test mass to optical bench (both on SC 1)
- optical bench on SC 1 to optical bench on SC 2
- optical bench to test mass (both on SC 2)

Their general functions are described below, where the specifications were an outcome of a design iteration that calculated the power spectral density of the noise as presented in the Section 4.1 and shown in Fig. 5, to which the reader is referred for a justification.

Test mass to optical bench The distance measurement between the test mass and the optical bench relies on obtaining the phase shift between two laser beams (red and green) as depicted in Fig. 4. An acousto-optic modulator (AOM) splits the laser light into two beams with two different frequencies f_1 and f_2 separated by few MHz (this frequency separation of MHz was chosen to avoid interference with Doppler shifts due to the natural relative movement of the spacecrafts). The beam with frequency f_1 is reflected from the test mass and sent to the measurement photo detector where it interferes with the beam of frequency f_2. The second beam f_2 has a fixed optical path and thus can be used as a reference signal to suppress common noise sources. The interference of the two beams generates a heterodyne signal (beat note) with a frequency $f_1 - f_2$. A phase meter is then used to measure the phase changes of the signal which is proportional to the displacement of the test mass.

Optical bench to optical bench In SC1 a frequency stabilized laser (master) sends light (10 W) to SC2. On SC2 the incoming beam interferes with the local laser. The signal is used to phase lock the laser on board to f_2 (around 10 MHz). The frequency f_2 was chosen to be above the induced Doppler shift of ± 3 MHz due to relative motion of the satellite (± 1.5 m/s) and also assures that the signal stays within the photodiodes and phase meter bandwidth. The locked laser on SC2 sends light back to SC1 with 10 W of power. The incoming beam from SC2 interferes with the laser at SC1 generating a beat note signal at f_2, which after correcting for the Doppler shift contains a phase delay (as measured by a phase meter) due to a passing gravitational

wave. The power and telescope diameter are chosen to allow for the design sensitivity. The design choices are elaborated in the noise analysis.

Three spacecraft configuration A minimal Michelson interferometer requires at least two arms to detect gravitational waves. In order to reduce the noise, and to obtain information on the polarization of the gravitational waves, GLINT is designed to have a total of three arms (see Fig. 4). In this setup, each spacecraft hosts two test masses, whose motion is tracked with respect to the test masses on either side of the arm. For the post-processing the distance between the spacecrafts is required, as the arm-length mismatch between the spacecraft changes how the laser frequency noise couples into the measurement and thus degrades the measurement. Henceforth, the distance between the spacecraft has to be known to within 1 cm, which can be achieved with satellite laser ranging, as further detail in Section 4.1. This knowledge allows us to perform Time Delay Interferometry (TDI) [78] as developed for LISA, which is done in post-processing by a combination of time delayed linear combinations of the signals as described in Section 7.1.

The three spacecraft that comprise GLINT allow us to use three interferometers (SC1-SC2-SC3, SC2-SC1-SC3 and SC3-SC1-SC2) see Fig. 4. This yields a better
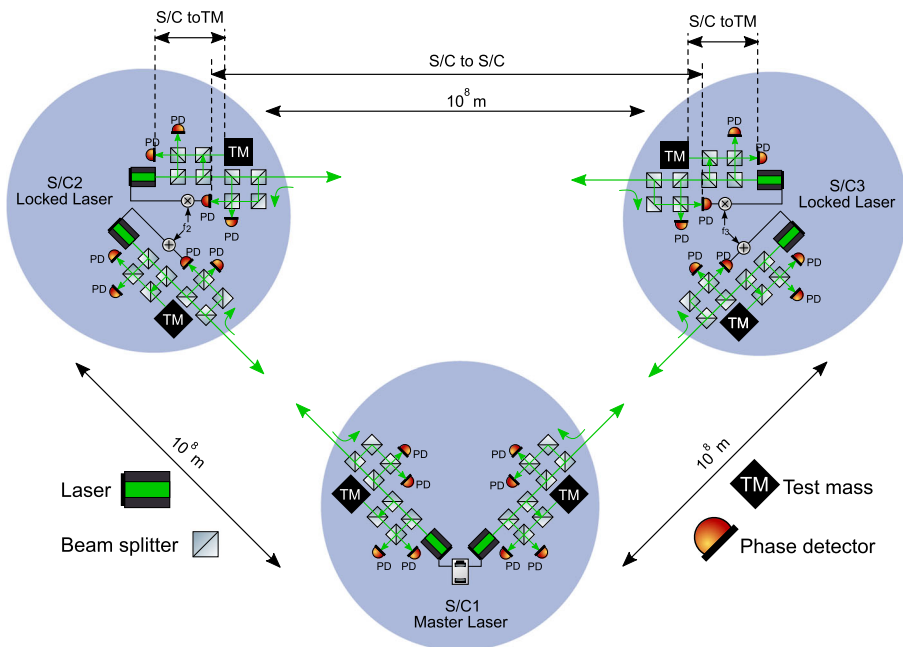

Fig. 4 Michelson Interferometer measurement concept to determine the distance changes between the test masses integrated into the optical bench. The "measurement detector" measures the phase changes caused by motion of the test mass while the reference detector is used as a reference to minimize common noise. Each spacecraft link requires a full setup with two linked test masses, resulting in a total of six test masses split on the three spacecraft

angular resolution, where the exact improvement depends on the source strength and location [25]. Additionally, the two separate laser links can discriminate between different gravitational wave polarizations [17]. As an example, let's consider a gravitational wave propagating along a direction perpendicular to the plane in which GLINT is contained. The sides of the triangle formed by the three freely-floating masses will be modified by the passage of a gravitational wave. The polarization of the GW can be inferred from the relative change in length of the sides of the triangle with respect to the others.

4.1 Noise analysis

As explained in Section 2.2 a sensitivity of $\delta h = 5 \times 10^{-24} 1/\sqrt{\text{Hz}}$ in the frequency range $0.01 - 1$ Hz is required. All noise levels must be designed to be of equal or less magnitude to assure the design sensitivity.

First we consider the performance of the interferometric measurement system. There are multiple noise sources that are indistinguishable from an actual displacement due to a gravitational wave. In the high frequency regime (around 1 Hz) the transfer function is the limiting factor, which is proportional to the arm length, L_{arm}, and the frequency, f, : $TF = |4.45 \times 10^{24} \ sinc(\pi \ L_{arm} \ f/c)|1/\sqrt{\text{Hz}}$ [18]. It describes how the gravitational waves couple to our instrument. To assure the required sensitivity at the 1 Hz level, GLINT, requires an arm length $L_{arm} = 100\,000$ km, as seen by the golden line in Fig. 5.

For the medium frequency (0.1 Hz to 1 Hz), shot noise deteriorates the interferometric measurement and drives the design. This noise source accounts for the fluctuations in the detected photon rate and the relative intensity noise, caused by fluctuations in the emitted laser power [63]. This is displayed by dashed orange line
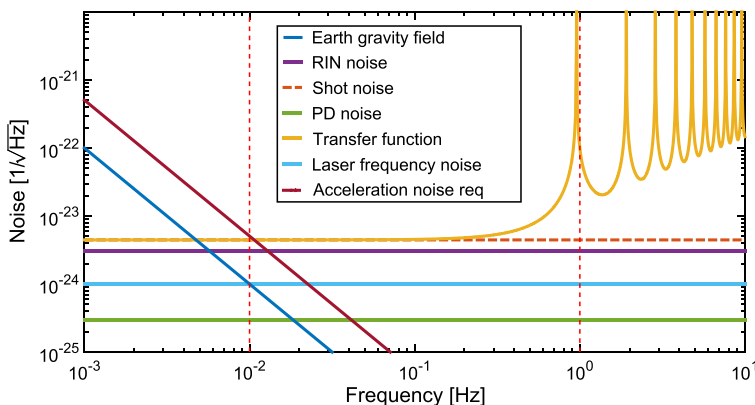

Fig. 5 GLINT sensitivity curve including the most important sources of noise. The purple line refers to the relative-intensity, the orange dash line indicates the shot noise for the given power of the laser. Photon detection noise is indicated by the green line, whereas the transfer function couples the arm length of oberservatory to the gravitational waves wavelength. Laser frequency noise is produced by flucations in the laser, and together with the shot noise and the RIN produces the total Read-Out noise. Lastly, the acceleration noise, is a combination of external, parasite acceleration

in Fig. 5. To keep this noise source below the threshold, a received power of 0.013 W is required. At lower received powers, the measurement noise would dominate the retrieval. From this minimum received power the combination of emitted power and telescope diameter can be obtained, where both can freely be chosen. The current iteration agreed on a combination of a 10 W laser with a 1.5 m diameter telescope. By calculating the Gaussian beam with an effective width of 1.35 M, and a misalignment of 1×10^{-7} rad, a received power of 0.013 W was assured. The Relative-Intensity Noise (RIN), was assumed to be 3×10^{-9} at MHz frequencies, is sent through the link and received by a 1.5 m diameter telescope.

The frequency noise of the lasers couples into phase fluctuations in the signal read-out. That is why one master laser is pre-stabilized by a reference cavity, to a level of $\delta\nu = 5$ Hz/$\sqrt{\text{Hz}}$, which is one order of magnitude better than LISA and current technology [59]. All the other lasers will be actively offset phase locked to the master laser. Even considering advanced technology, further noise suppression is needed to achieve the required sensitivity. This is done with time-delay interferometry [78], which can further reduce the frequency noise based on the positional knowledge, by minimizing the product of measurement uncertainty and laser frequency noise [45]. The combination of $\delta\nu = 5$ Hz/$\sqrt{\text{Hz}}$ and 1 cm was found to be a reasonable given current technology [28, 59]. An improvement in one technology, can be used to relax the requirement on the complementary technology.

In addition, the optical bench requires a thermal stability of $\delta T = 0.1\,\mu\text{K}/\sqrt{\text{Hz}}$ in order to maintain the optical path length errors within the requirements. The acceleration noise is derived from thermal pressure based on [51], by redoing the calculations for GLINT design parameters. The Brownian noise induced through residual pressure in the test chamber [12, 23], in combination with the thermal stability are among the most challenging requirements for the concept, and require further in-depth study to mitigate their noise contribution.

Finally, the noise levels of the phase meter need to be $\delta\phi = 10^{-9}$ rad/$\sqrt{\text{Hz}}$. Note that all the requirements only apply to the measurement band of the mission, from 0.01 - 1 Hz [17].

In the low frequency band around 0.01 Hz the quality of the test mass free fall determines the performance. All residual forces acting on the test masses induce an acceleration noise that mimics the effect of a gravitational wave. The requirement for this noise source is $\delta a = 10^{-18}$ m/(s$^2\sqrt{\text{Hz}}$), to achieve a the design strain at 0.01 Hz according to the following relation: $\delta h = (2*\pi/f)^{-2}*1/L_{arm}*\delta a$ [18, 45]. This is three orders of magnitude better than current LISA Pathfinder performance [12], and presents a major challenge for concept and requires significant advancement.

Thermal radiation due to temperature differences, and radiation pressure exerted by the laser power sent to the mass are minimized to the requirement by using a cubic test mass of 7 kg and side-length 7 cm (Au-Pt alloy - density 2×10^4 kg/m^3). The pressure in the mass assembly needs to be kept at $3 \cdot 10^{-7}$ Pa and a temperature of around 293 K within a thermal stability of $\delta T = 0.1\,\mu\text{K}/\sqrt{\text{Hz}}$ based on equation 7 by [51]. This is above the stability achieved on LISA Pathfinder of 10 to 50 $\mu\text{K}/\sqrt{\text{Hz}}$ [12].

Magnetic forces need to be attenuated by a magnetic shielding at the test masses, whose magnetic susceptibility and magnetic momentum are required to be $\chi_{\text{mag}} = 10^{-7}$ and $m_r = 10^{-7}$ A m^2 to reduce the magnetic noise below the level of significance.

These numbers are based on LISA requirements [10], however, require further improvement to about 2 orders of magnitude from LISA design. Finally, the frequency band of the actuators (thrusters) needs to be shifted away to lower frequencies than the measurement band.

Figures 1 and 5 illustrate the influence of the mentioned noise errors in the sensitivity of the instrument. In summary, in the high frequencies the sensitivity drops due to the transfer function of the interferometer. At intermediate frequencies the shot noise is the limiting error source. At low frequencies the acceleration noise limits the sensitivity.

4.2 Orbit

The three satellites will be placed in circular orbit (r = 57 735 km) around Earth to form an equilateral triangle with an an armlength of 100 000 km as depicted in Fig. 6. The constellation can be formed with a single launch by a rocket similar in performance and fairing to the current Ariana 5 ECA or the Falcon Heavy [69]. The inclination of the target orbit does not follow stringent requirements as long the orbital plane does not coincide with the ecliptic to reduce the occurrence of direct light hitting the telescope. Hence, the target inclination can be chosen to minimize the launch cost for a given launch site.

A separation of more than 5° from the ecliptic allows for continuous operation of the telescope throughout the year apart from a two week period twice a year. During this time the telescope would be facing the sun directly and thus active avoidance is required by turning the satellites out of the sun. Furthermore, at this altitude the inhomogeneous gravity field only has a minor impact on the satellites and thus by using AGI System Tool Kit's (STK) High-Precision Orbit Propagator (HPOP) which makes use of the full gravitational model (including the lunar influence), one finds that the angle of 60° between the arms changes only by about 0.04°. The changes in angle can be accomodated by using steerable mirrors to focus the beam onto the other spacecraft, and raster scans can be employed to improve the pointing of the spacecraft. Using STK it was estimated that 10 m/s is sufficient for orbit maintenance

Fig. 6 Sketch of the proposed launch and orbit
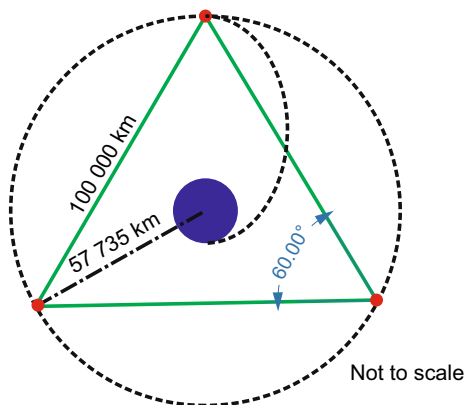
per year per spacecraft. After the mission is finished there is no need for disposal as the orbit is beyond the protected geostationary orbit belt (42 164 km).

5 Technological challenges

To reach a strain sensitivity of $10^{-24}\ 1/\sqrt{\text{Hz}}$ there are a number of challenges which need to be solved. The most difficult of these challenges are outlined below, however, many more exists and must be included in a more detailed analysis, which is beyond the scope of this article:

- A phase read-out technique which can resolve phase differences of the order $10^{-9}\ \text{rad}/\sqrt{Hz}$ for a heterodyne beat note at MHz frequencies. This is three orders of magnitude better than the current best possible systems [21].
- The test mass for GLINT is required to have a mass of 7 kg. The use of a such a heavy test mass requires significant changes to the caging mechanism which releases the test mass once the satellites have reached their final orbits without damaging the enviroment [85].
- Current state of the art manufacturing techniques and the use of expansive ultra-low-expansion materials allow us to build quasi-monolithic centimeter scale objects with a fractional long-term stability of approximately $10^{-13}\ 1/\sqrt{\text{Hz}}$ (at moderate temperatures) [71]. The ultra-low-expansion material is required for the optical test bench, to avoid parasitic movement. For GLINT this needs to be improve at least three orders of magnitude. Such materials do not yet exist.

It is impossible to estimate the cost or time-scale necessary for these developments in detail, as they will likely require new technologies. Future research will detail if those developments are even possible on a fundamental level. The above mentioned sources will mostly likely change our understanding of the universe. However, to study these sources major innovation will be required in order to either: (i) improve existing technology to the level we have outlined or (ii) identify another method of measuring gravitational waves which can achieve the required sensitivity.

6 Spacecraft design

This section elaborates on the detailed design of the individual subsystems and their corresponding design drivers.

6.1 Mass and power budget

Table 2 shows the mass and power budgets calculated for each satellite. System margins of 20% have been included to account for the readiness of the technology. Each satellite has a total mass of 1598 kg including the propellant. The payload is the largest contribution to the overall mass as this includes both the telescope and the optical truss. Moving onto the power budget, the total power needed is 1134 W. This covers nominal operation plus losses and battery charging for the short eclipse times.

The primary power source is solar power, for which body mounted solar cells are used. The solar panel size to be illuminated directly is 5.069 m^2, which accounts for several efficiency factors including solar panel efficiency, thermal efficiency and degradation. Lithium Ion batteries were sized to survive and operate for the duration of the longest eclipse: 1.45 h during the 38.35 h orbit. The mode requiring the most power is the science mode, during which the energy intense lasers will be active.

6.2 Structural design

The spacecraft are designed to be 4.5m wide (diameter) and 3m tall. The structural design of the GLINT spacecraft as shown in Fig. 7, is composed of three main parts: the main structures, the payload section, and side panels. The main structures occupy the lower part of the spacecraft. It contains the main frame that supports a composite sandwich structural plate. The main frame endures most of the dynamic loads (vibration excitation and shocks) during the launch and the thrust loads during cruise. It is equipped at its bottom with apogee thrusters and their hydrazine tank, a laser unit and several components of the service module (electronics and data processing units). Four composite compression cylinders link the structural frame to the hexagonal interface on the top panel.

The payload section is mounted on top of the main frame structural plate. It is composed of composite materials and constitutes a stable support for the primary and secondary mirrors, with mechanical and thermal strains in the picometer range. Located inside the torus is the suspended optical bench, with the test mass at its center. The beams that are connecting the torus and the optical bench, are designed to reduce the thermal strain on the optical bench. The side sandwich panels are covered with multi-layers insulation to limit the thermal cycling of the payload. On the outside of the side panels, the solar panels are attached to provide power and also serve as the base for the attitude and orbit control system, including the thrusters and star trackers.

The main advantage of this structural architecture is that it decouples the noisy service module from the payload. Mechanical disturbances coming from the thrusters are carried by the main frame, the compression cylinders, and the side panels. The noise translated from the service module to the torus and the optical bench is reduced by long load path as provided by the beams and compression cylinders. The thermal

Table 2 Mass and Power budgets (Note 20% contingencies included)

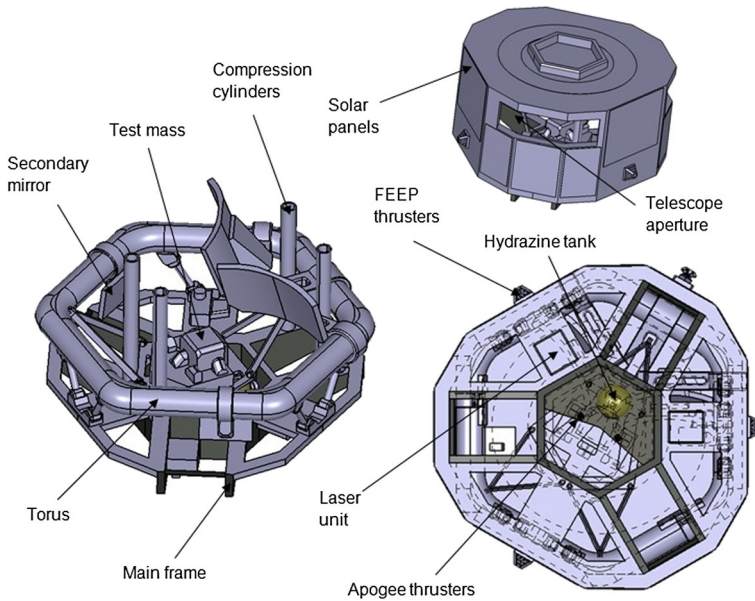| Mass budget		Power budget	
Component	Mass (kg)	Component	Power consumption (W)
Dry mass	1269	Payload	350
Propellant	63	Platform	595
Wet mass	1332	Required power	945
System margin 20%	266	System margin 20%	189
Total mass	1598	Total power	1134

Fig. 7 Preliminary design of the spacecraft. The first design iteration included rectangular mirrors, where the second iteration updated to circular mirror for manufacturing purposes

gradients at the payload level are also limited by having the heat dissipative elements (laser unit, electronics) mounted at the back of the structural plate and thus outside the payload compartment.

6.2.1 Telescope design

The telescope design includes six silicone carbide mirrors. The current design iteration is based on flight proven hardware similar to the used in the GAIA spacecraft [32]. The chosen primary mirror has a radius of curvature of 0.75m with a diameter of 1.5 m. Whereas the GAIA design used circular mirrors, GLINT aims at employing circular mirror to facilitate production. The overall stability of the telescope is of paramount importance and thus the detailed design must account for it. Variations in the position of the two primary and secondary mirrors as well as the suspended test mass unit are precisely computed using secondary lasers. The beams are focused on those optical elements and the phase of the reflected beams is sensed using interferometry and gives accurate data about the telescope displacements. This information is then processed by the data processing unit to remove the parasite contribution of the optical setup's motion from the science measurement.

6.3 Thermal subsystem

The spacecraft is exposed to several heat sources: solar radiation, Earth reflection, infrared radiation from Earth and internally dissipated electrical energy. Thermal

design is required to maintain the optimal temperature of the spacecraft. Due to time constraints, only estimates were included to define the temperature of the spacecraft [46]; in the hot case it is kept at 25 °C. Due to the large thermal mass and black multi layer insulation the average temperature is maintained at 22 °C during the maximum eclipse of 70 minutes, where heaters are employed to maintain the temperature, if it drops below this threshold.

The payload itself requires a thermal stability of 0.1 μK/$\sqrt{Hz}$ at a frequency of 10^{-2} Hz. While this may be a challenging requirement, temperature noise decreases rapidly with increasing frequency and thus is considered an achievable requirement. Heaters, thermal isolation and structural materials with a small thermal expansion coefficient are used to maintain this. Detailed designs studies have to be performed to determine this performance.

6.4 Propulsion system

A satellite is exposed to various external accelerations which reduce the accuracy of the measurements. Noise sources include residual air drag, radiation pressure, micrometeorite impacts, solar wind and other small forces that act on its surface. Using drag-free control will cancel these non-gravitational forces to acceptable levels in order to provide a dynamically quiet platform for high-precision experiments [36].

The concept of drag-free control is assured by the following condition. The test mass is unsupported and protected from outside disturbances. Secondly, the path of the satellite is purely gravitational. Thirdly, the thrusters produce forces equal and opposite to the disturbances and thus are a measure of these external disturbances with improved bandwidth and accuracy compared with measuring the effect on a satellite's orbit [27].

Micropropulsion thrusters In order to provide a high-precision measurement in the spacecraft, it is required to have a thrust precision of at least 0.5 μN and a thrust noise of 0.1 μN/$\sqrt{Hz}$ and a thrust range of 100 μN to based an article on the propulsion options for the LISA Mission [22]. From the few suitable options, the best candidate for this mission design are the Field-Emission Electric Propulsion (FEEP) thrusters, due to their advanced control and mature development state with demonstration scheduled for 2017.

FEEP is an advanced electrostatic space propulsion concept, a form of ion thruster, that uses liquid metal (usually either cesium, indium or mercury) as a propellant. A potential difference of the order of 10 kV is applied between electrodes, which generates a strong electric field at the tip of the metal surface. At sufficiently high values of the applied field, ions are extracted from the tip and are accelerated to high velocities (typically 100 km/s or more) [56, 76]. FEEPs have been matured over recent years by private companies such as Fotec GmbH/AMR Propulsion Innovations GmbH, which provided the technical details for their plug-and-play system (see Table 3).

6.5 Attitude and orbit control system

Based on the constellation design a 0.35 mrad pointing accuracy has to be achieved, this requirement is given from the breathing angle as identified by the constellation design (Section 4.1). The pointing knowledge is obtained by the use of a 3 headed star tracker and the accuracy is accomplished by relying on the same FEEPs as described above. Furthermore, to comply with the fine pointing of the laser beam the system relies on differential wave front sensing. The natural breathing angle will cause the beam to lose lock with the spacecraft, so that fine pointing of the laser beams is required below the beam divergence of 0.3 μrad. Using a piezo controller on the mirror, based on the Beam Steering Mirror on Herschel [62], it is possible to achieve a 0.1 μrad pointing accuracy. In case of safe mode, the attitude is detected by two sun sensors and an Inertial Measurement Unit (IMU). For attitude control the three stacks of FEEP thrusters are used. Every stack consists of four thrusters together, providing torque-free and pure torque control.

6.6 Data handling

The command and data handling subsystem performs two major functions. It receives, validates, decodes and distributes commands to other spacecraft systems and also gathers, processes, and formats spacecraft housekeeping and mission data for down-link or use by an on-board computer. Temporary storage of the data is needed as well as access to a flexible on-board computer. Therefore, each of the spacecraft data handling architecture is estimated in this preliminary phase based on the Thales Leonardo architecture with an estimated power consumption of 33 W and a mass of 10.2 kg, including internal redundancy. The main tasks of the on-board computer are decoding of the telecommands from the ground and ensuring their execution, on-board housekeeping and scientific data telemetry formatting for transmission, overall data management, execution of the attitude, and orbit control system software. The internal mass memory of 32 GB (end of life) is sized for storing housekeeping and payload data. Due to the low data volume of 0.6 GB (estimated later in the section) per spacecraft per day, no additional units are required and the design foresees to incorporate the internal mass memory directly into the command and data

Table 3 Specifications of FEEP thrusters as obtained from Fotec GmbH

Thrust, range per unit	0.3-150 μN
Propellant	In
Thrust Accuracy	0.1 μN
Thrust Response	0.1 ms
Thrust Noise	$<0.1 \, \mu\text{N}/\sqrt{\text{Hz}}$
Specific Impulse	4000-8000 s
System Weight	>14 kg
Lifetime	>15000 h
Thrust Control	Accelerate voltage

management unit. Lastly, the system is compatible with the radiation environment in GEO type orbits.

6.7 Telecommunication

The Telemetry Tracking & Control subsystem is dedicated to the retrieval of telecommands and the transmittance of telemetry. The telemetry data consists of the science data, spacecraft or payload operations and housekeeping data of the subsystem including information on voltages, currents, pressures, temperature, operational states, etc. The scientific data acquired by the payload of the spacecraft is down-linked to the ground stations.

Data volume The net effective continuous data rate for each instrument of the constellation is 57 kbps of which 15 kbps is housekeeping data [46] and 42 kbps is science data, based on estimates of LISA [14]. The daily data volume is therefore estimated to be 0.6 GB per spacecraft per day, making this a non critical subsystem. It is established that every day one spacecraft has a downlink opportunity, so that individual spacecraft downlink a data volume of 1.8 GB every third day. The low ground velocity and the spacing of the spacecraft for an assumed inclination of 5° (for a launch from Kourou), results that 17 hours per day any of the three spacecraft is in view of the ground station. Assuming a downlink window of 2 hours, the data rate of 2048 kbps is sufficient to downlink the given data. No on-board reduction of the data is required.

Communication The requirement for the scientific data downlink, resulted in the choice of X-band antenna, compatible with the Deep Space Antenna network. To avoid excessive reorientation for communication each of the spacecraft will carry three independent patch antennas to cover provide better coverage. The calculated link margin is 8.77 dB based on 5 W transmission power. Furthermore, a set of redundant omnidirectional UHF antennas is installed on every satellite to provide communication capabilities during safe mode assuring that contact with the spacecraft can be established at all time.

7 Ground segment infrastructure

The ground segment provides capabilities for monitoring and controlling the spacecraft and payload during all phases of the mission, as well as for the reception, archiving and distribution of the data gathered by the payload instruments. For the GLINT mission the ground segment consists of a ground station to receive the data, a mission operation center to control the spacecraft and a science operation center to process the scientific data. For these tasks the existing ESA ground segment elements and facilities are used. The communication and tracking operations are established with ESA's 35 m ground stations, such as the antenna in Malargüe (Deep Space Antenna DSA 3) which is part of the European Deep Space Network. The 35 m station provides the improved range, radio technology and data rates required by current
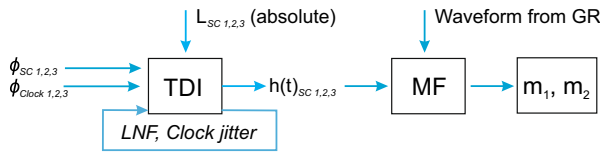
Fig. 8 Post Processing Algorithm. Time Delay Interferometry (TDI) cancels the laser frequency noise (LNF) and the clock jitter. This is accomplished by combining the phase measurements of the spacecraft (ϕ_{SC}), the phase of the clock (ϕ_{clock}) and range information (L) by different spacecrafts. The recovered time-dependent strain (h) is then compared to expected waveforms from General Relativity (GR) in a process called Matched Filtering (MF)

and next-generation exploratory missions. The Mission Operations Centre will be located at European Space Operations Centre in Darmstadt, Germany.

7.1 Post processing

To maximize the scientific output the measured strains are corrected for known error sources. For instance, due to relative movements between the spacecraft, the distance of the interferometer arm is expected to change by approximately ±0.03% over one orbit. As a consequence, the resulting unequal arm configuration of GLINT turns laser frequency into additional noise, which could impede the scientific performance of the mission. There are three approaches to reduce the noise to the required sensitivity: pre-stabilization, arm locking and time delay interferometry (TDI) [50]. With TDI we can cancel laser frequency noise (LNF) and clock jitter by combining the phase measurements made at different times. Matched filtering can be used as a next step at it can recognize signals of an expected form. An example of how it can be done can be seen in Fig. 8 based on Bender [20].

The required timing of the measurement is set by the light travel time between the GLINT spacecraft. Using current technology, the accuracy of 1 cm corresponding to 33 ps to meet the laser frequency noise suppression requirement can be obtained. The excellent positional knowledge of the satellites and the short round-trip time of the signal in earth orbit make arm locking a minor challenge. For further information see Shaddock et al. [74] and Armstrong et al. [13].

8 Conclusions

The measurements made by GLINT will provide extensive data on black holes, which will decrease the parameter space for the models of formation and evolution of these large massive objects. The gravitational region to be studied has never been directly observed before, and this mission will fill in these blanks.

Utilizing gravitational waves for studying the universe rapidly widens the measurement range and will have an extensive impact on the research within fundamental physics and astrophysics, as well as corroborate our current view of the universe that has been obtained by electromagnetic radiation.

The engineering aspects of the GLINT project are very challenging since they require advanced technologies to limit the noise in the instruments. Even if those technologies need to be improved in order to give an answer to the requirements made, this work paves the way for a promising future in gravitational wave detection by identifying the potential sources of error in the measurement process and quantifying them thoroughly. Various trade-offs have been made in order to identify key technologies to cope with the high accuracy required and to judge the technological readiness level of the instruments studied. This study has also developed concepts for constellation flight of satellites and a new structural design for spacecraft.

References

1. Aasi, J. et al.: Advanced LIGO. Class Quant Grav **32**, 074,001 (2015). https://doi.org/10.1088/0264-9381/32/7/074001, arXiv:1411.4547

2. Acernese, F. et al.: Advanced virgo: a second-generation interferometric gravitational wave detector. Class Quant Grav **32**(2), 024,001 (2015). https://doi.org/10.1088/0264-9381/32/2/024001. arXiv:1408.3978

3. Adam, R. et al.: Planck 2015 results. I. Overview of products and scientific results. Astron Astrophys **594**, A1 (2016). https://doi.org/10.1051/0004-6361/201527101. arXiv:1502.01582

4. Alexander, K.D., Wieringa, M.H., Berger, E., Saxton, R.D., Komossa, S.: Radio observations of the tidal disruption event XMMSL1 j0740 85. apj **837**, 153 (2017). https://doi.org/10.3847/1538-4357/aa6192, arXiv:1610.03861

5. Alves, M.E.S., Moraes, P.H.R.S., de Araujo, J.C.N., Malheiro, M.: Gravitational waves in $f(r,t)$ and $f(r,T^{\phi})$ theories of gravity. Phys Rev D **94**, 024,032 (2016). https://doi.org/10.1103/PhysRevD.94.024032

6. Amaro-Seoane, P., Aoudia, S., Babak, S., Binétruy, P., Berti, E., Bohé, A., Caprini, C., Colpi, M., Cornish, N.J., Danzmann, K., Dufaux, J.F., Gair, J., Jennrich, O., Jetzer, P., Klein, A., Lang, R.N., Lobo, A., Littenberg, T., McWilliams, S.T., Nelemans, G., Petiteau, A., Porter, E.K., Schutz, B.F., Sesana, A., Stebbins, R., Sumner, T., Vallisneri, M., Vitale, S., Volonteri, M., Ward, H.: Low-frequency gravitational-wave science with eLISA/NGO. Classical and Quantum Gravity **29**(12), 124016 (2012). https://doi.org/10.1088/0264-9381/29/12/124016. arXiv:1202.0839

7. Amaro-Seoane, P., Aoudia, S., Babak, S., Binétruy, P., Berti, E., Bohe, A., Caprini, C., Colpi, M., Cornish, N.J., Danzmann, K., et al.: Low-frequency gravitational-wave science with elisa/ngo. Classical and Quantum Gravity **124**(12), 016 (2012)

8. Ando, M., Kawamura, S., Seto, N., Sato, S., Nakamura, T., Tsubono, K., Takashima, T., Funaki, I., Numata, K., Kanda, N., et al.: Decigo and decigo pathfinder. Classical and Quantum Gravity **084**(8), 010 (2010)

9. Armano, M., Benedetti, M., Bogenstahl, J., Bortoluzzi, D., Bosetti, P., Brandt, N., Cavalleri, A., Ciani, G., Cristofolini, I., Cruise, A., et al.: Lisa pathfinder: the experiment and the route to LISA. Classical and Quantum Gravity **26**(9), 094,001 (2009)

10. Armano, M., Audley, H., Auger, G., Baird, J., Binetruy, P., Born, M., Bortoluzzi, D., Brandt, N., Bursi, A., Caleno, M., et al.: Disentangling the magnetic force noise contribution in LISA Pathfinder. J. Phys. Conf. Ser. **610**(1), 012024 (2015)

11. Armano, M., Audley, H., Auger, G., Baird, J., Bassan, M., Binetruy, P., Born, M., Bortoluzzi, D., Brandt, N., Caleno, M., Carbone, L., Cavalleri, A., Cesarini, A., Ciani, G., Congedo, G., Cruise, A., Danzmann, K., de Deus Silva, M., Rosa, R.D., Diaz-Aguiló, M., Fiore, L.D., Diepholz, I., Dixon, G., Dolesi, R., Dunbar, N., Ferraioli, L., Ferroni, V., Fichter, W., Fitzsimons, E., Flatscher, R., Freschi, M., Marín, A.G., Marirrodriga, C.G., Gerndt, R., Gesa, L., Gibert, F., Giardini, D., Giusteri, R., Guzmán, F., Grado, A., Grimani, C., Grynagier, A., Grzymisch, J., Harrison, I., Heinzel, G., Hewitson, M., Hollington, D., Hoyland, D., Hueller, M., Inchauspé, H., Jennrich, O., Jetzer, P., Johann, U., Johlander, B., Karnesis, N., Kaune, B., Korsakova, N., Killow, C., Lobo, J., Lloro, I., Liu, L., López-Zaragoza, J., Maarschalkerweerd, R., Mance, D., Martín, V., Martin-Polo, L., Martino, J., Martin-Porqueras, F., Madden, S., Mateos, I., McNamara, P., Mendes, J., Mendes, L., Monsky, A., Nicolodi, D., Nofrarias, M., Paczkowski, S., Perreur-Lloyd, M., Petiteau, A., Pivato, P., Plagnol, E., Prat, P., Ragnit, U., Raïs, B., Ramos-Castro, J., Reiche, J., Robertson, D., Rozemeijer, H., Rivas, F., Russano, G., Sanjuán, J., Sarra, P., Schleicher, A., Shaul, D., Slutsky, J., Sopuerta, C., Stanga, R., Steier, F., Sumner, T., Texier, D., Thorpe, J.I., Trenkel, C., Tröbs, M., Tu, H., Vetrugno, D., Vitale, S., Wand, V., Wanner, G., Ward, H., Warren, C., Wass, P.J., Wealthy, D., Weber, W., Wissel, L., Wittchen, A., Zambotti, A., Zanoni, C., Ziegler, T., Zweifel, P.: Sub-femto-g free fall for space-based gravitational wave observatories: Lisa pathfinder results. Phys. Rev. Lett. **116**(23) (2016). https://doi.org/10.1103/PhysRevLett.116.231101. http://eprints.gla.ac.uk/119966/

12. Armano, M., Audley, H., Auger, G., Baird, J., Bassan, M., Binetruy, P., Born, M., Bortoluzzi, D., Brandt, N., Caleno, M., et al.: Sub-femto-g free fall for space-based gravitational wave observatories: Lisa pathfinder results. Phys. Rev. Lett. **116**(23), 231,101 (2016)

13. Armstrong, J., Estabrook, F., Tinto, M.: Time Delay Interferometry. http://www.aei.mpg.de/pau/GWs_Course/data/L34.pdf (2002)

14. Audley, H., Babak, S., Baker, J., Barausse, E., Bender, P., Berti, E., Binetruy, P., Born, M., Bortoluzzi, D., Camp, J., et al.: Laser interferometer space antenna. arXiv:170200786 (2017)

15. Backer, D.C., Hellings, R.W.: Pulsar timing and general relativity. araa **24**, 537–575 (1986). https://doi.org/10.1146/annurev.aa.24.090186.002541

16. Backer, D.C., Jaffe, A.H., Lommen, A.N.: Massive black holes, gravitational waves and pulsars. Coevolution of black holes and galaxies. p. 438 (2004)

17. Barke, S.: Inter-spacecraft frequency distribution for future gravitational waves observatories. PhD thesis (2015)

18. Barke, S., Wang, Y., Delgado, J.E., Tröbs, M., Heinzel, G., Danzmann, K.: Towards a gravitational wave observatory designer: sensitivity limits of spaceborne detectors. Classical and Quantum Gravity **32**(9), 095,004 (2015)

19. Begelman, M.C.: Accreting black holes. arXiv:1410.8132 (2014)

20. Bender, P.: LISA: laser interferometer space antenna for the detection and observation of gravitational waves: pre-phase a report. Max-Planck-Institut fur Quantenoptik (1998)

21. Bykov, I., Delgado, J.JE., Marín, A.FG., Heinzel, G., Danzmann, K.: LISA: Phasemeter development: advanced prototyping. J. Phys. Conf. Ser. **154**, 012017 (2009). IOP Publishing

22. Cardiff, E., Marr, G.: Propulsion options for the lisa mission. In: 40th AIAA/ASME/SAE/ASEE joint propulsion conference and exhibit, p. 3440 (2004)

23. Cavalleri, A., Ciani, G., Dolesi, R., Heptonstall, A., Hueller, M., Nicolodi, D., et al.: Increased brownian force noise from molecular impacts in a constrained volume. Phys. Rev. Lett. **103**(14), 140601 (2009)

24. Cornish, N., Robson, T.: Galactic binary science with the new LISA design. arXiv:1703.09858 (2017)

25. Cutler, C.: Angular resolution of the lisa gravitational wave detector. Phys. Rev. D **57**(12), 7089 (1998)

26. Danzmann, K., et al.: LISA: Unveiling a hidden universe. assessment study report (2011)

27. DeBra, D.B.: Drag-free spacecraft as platforms for space missions and fundamental physics. Classical and Quantum Gravity **14**(6), 1549 (1997). http://stacks.iop.org/0264-9381/14/i=6/a=026

28. Degnan, J.J.: Millimeter accuracy satellite laser ranging: a review. Contributions of space geodesy to geodynamics: technology (pp. 133–162) (1993)

29. Dimmelmeier, H., Font, J., Janka, H.T., Marek, A., Müller, E., Ott, C.: Max Planck Institute for Astrophysics Waveform Catalogue. http://www.mpa-garching.mpg.de/rel_hydro/wave_catalog.shtml, [Accessed 30-August-2015] (2015)

30. Dooley, K.L.: Status of GEO 600. J Phys Conf Ser **610**(1), 012,015 (2015). https://doi.org/10.1088/1742-6596/610/1/012015, arXiv:1411.6588

31. Eilers, A.C., Davies, F.B., Hennawi, J.F., Prochaska, J.X., Lukić, Z., Mazzucchelli, C.: Implications of z 6 quasar proximity zones for the epoch of reionization and quasar lifetimes. Astrophys. J. **840**(1), 24 (2017)

32. Erdmann, M., Sarri, G.: GAIA Mirrors ready to shine, http://sci.esa.int/gaia/49199-gaia-mirrors-ready-to-shine/

33. Flanagan, E.E., Hughes, S.A.: Measuring gravitational waves from binary black hole coalescences. i. signal to noise for inspiral, merger, and ringdown. Phys. Rev. D **57**(8), 4535 (1998)

34. Flanagan, E.E., Hughes, S.A.: Measuring gravitational waves from binary black hole coalescences. ii. the waves' information and its extraction, with and without templates. Phys. Rev. D **57**(8), 4566 (1998)

35. Fryer, C.L., Holz, D.E., Hughes, S.A.: Gravitational wave emission from core collapse of massive stars. ApJ **565**, 430–446 (2002). https://doi.org/10.1086/324034. arXiv:astro-ph/0106113

36. Funakki, I., Nakayama, Y.: Micro-thruster options for the japanese space gravitational wave observatory missions. In: IEPC, Presented at the 32nd International Electric Propulsion Conference, vol. 308 (2011)

37. Gair, J.R., Babak, S., Sesana, A., Amaro-Seoane, P., Barausse, E., Berry, C.P., Berti, E., Sopuerta, C.: Prospects for observing extreme-mass-ratio inspirals with LISA. arXiv:1704.00009 (2017)

38. Hannam, M., et al.: The samurai project: Verifying the consistency of black-hole-binary waveforms for gravitational-wave detection. Phys. Rev. **D79**, 084,025 (2009). https://doi.org/10.1103/PhysRevD.79.084025, arXiv:0901.2437

39. Hobbs, G., Edwards, R., Manchester, R.: Tempo2, a new pulsar timing package. 1. overview. Mon. Not. Roy. Astron. Soc. **369**, 655–672 (2006). https://doi.org/10.1111/j.1365-2966.2006.10302.x. arXiv:astro-ph/0603381

40. Hobbs, G., Archibald, A., Arzoumanian, Z., Backer, D., Bailes, M., Bhat, N.D.R., Burgay, M., Burke-Spolaor, S., Champion, D., Cognard, I., Coles, W., Cordes, J., Demorest, P., Desvignes, G., Ferdman, R.D., Finn, L., Freire, P., Gonzalez, M., Hessels, J., Hotan, A., Janssen, G., Jenet, F., Jessner, A., Jordan, C., Kaspi, V., Kramer, M., Kondratiev, V., Lazio, J., Lazaridis, K., Lee, K.J., Levin, Y., Lommen, A., Lorimer, D., Lynch, R., Lyne, A., Manchester, R., McLaughlin, M., Nice, D., Oslowski, S., Pilia, M., Possenti, A., Purver, M., Ransom, S., Reynolds, J., Sanidas, S., Sarkissian, J., Sesana, A., Shannon, R., Siemens, X., Stairs, I., Stappers, B., Stinebring, D., Theureau, G., van Haasteren, R., van Straten, W., Verbiest, J.PW., Yardley, D.RB., You, X.P.: The international pulsar timing array project: using pulsars as a gravitational wave detector. Classical and Quantum Gravity **27**(8), 084013 (2010). https://doi.org/10.1088/0264-9381/27/8/084013. arXiv:0911.5206

41. Hulse, R.A., Taylor, H.J.: Discovery of a pulsar in a close binary system. In: Bulletin of the american astronomical society, bulletin of the american astronomical society, vol. 6, p. 453 (1974)

42. Iwasawa, K., Fabian, A.C., Mushotzky, R.F., Brandt, W.N., Awaki, H., Kunieda, H.: The broad iron k emission line in the seyfert 2 galaxy IRAS 18325-5926. mnras **279**, 837–846 (1996). https://doi.org/10.1093/mnras/279.3.837

43. Kokkotas, K.D.: Gravitational wave astronomy (with 2 figures). In: Röser, S. (ed.) Reviews in modern astronomy, reviews in modern astronomy, vol. 20, p. 140 (2008). https://doi.org/10.1002/9783527622993.ch7, arXiv:0809.1602

44. La Mura, G., Busetto, G., Ciroi, S., Rafanelli, P., Berton, M., Congiu, E., Cracco, V., Frezzato, M.: Relativistic plasmas in AGN jets - from synchrotron radiation to γ-ray emission. arXiv:1702.06779 (2017)

45. Larson, S.L., Hiscock, W.A., Hellings, R.W.: Sensitivity curves for spaceborne gravitational wave interferometers. Phys. Rev. D **62**(6), 062,001 (2000)

46. Larson, W.J., Wertz, J.R.: Space Mission Analysis and Design. Tech. Rep., Microcosm Inc., Torrance (1992)

47. Laureijs, R., Amiaux, J., Arduini, S., Auguères, J., Brinchmann, J., Cole, R., Cropper, M., Dabin, C., Duvet, L., Ealet, A., et al.: Euclid Definition Study Report. arXiv:1110.3193 (2011)

48. LIGO Scientific Collaboration, VIRGO Collaboration: Observation of gravitational waves from a binary black hole merger. Phys. Rev. Lett. **116**, 061,102 (2016). https://doi.org/10.1103/PhysRevLett.116.061102

49. Liu, K., Verbiest, J.P.W., Kramer, M., Stappers, B.W., van Straten, W., Cordes, J.M.: Prospects for high-precision pulsar timing. mnras **417**, 2916–2926 (2011). https://doi.org/10.1111/j.1365-2966.2011.19452.x, arXiv:1107.3086

50. Livas, J., Thorpe, J., Numata, K., Mitryk, S., Mueller, G., Wand, V.: Frequency-tunable pre-stabilized lasers for LISA via sideband locking. Classical and Quantum Gravity **26**(9), 094,016 (2009)

51. Lobo, A., Nofrarias, M., Ramos-Castro, J., Sanjuán, J.: On-ground tests of the lisa pathfinder thermal diagnostics system. Classical and Quantum Gravity **23**, 5177–5193 (2006). https://doi.org/10.1088/0264-9381/23/17/005

52. Loeb, A., Maoz, D.: Using atomic clocks to detect gravitational waves. arXiv:150100996 (2015)

53. Lorimer, D., Kramer, M.: Handbook of Pulsar Astronomy. Cambridge Observing Handbooks for Research Astronomers, Cambridge University Press, https://books.google.pt/books?id=OZ8tdN6qJcsC (2005)

54. Madau, P., Haardt, F., Dotti, M.: Super-critical growth of massive black holes from stellar-mass seeds. ApJS **784**, L38 (2014). https://doi.org/10.1088/2041-8205/784/2/L38. arXiv:1402.6995

55. Manchester, R., Taylor, J.: Pulsars. A Series of books in astronomy and astrophysics, W. H. Freeman, https://books.google.pt/books?id=tcFlQgAACAAJ (1977)

56. Marcuccio, S., Genovese, A.: Experimental performance of field emission microthrusters. J. Propuls. Power **14**(5), 774–781 (1998). http://www.alta-space.com/uploads/file/publications/feep/Marcuccio-JPP14_5_1998.pdf

57. McClintock, J.E., Narayan, R., Davis, S.W., Gou, L., Kulkarni, A., Orosz, J.A., Penna, R.F., Remillard, R.A., Steiner, J.F.: Measuring the spins of accreting black holes. Class Quant. Grav. **28**, 114,009 (2011). https://doi.org/10.1088/0264-9381/28/11/114009. arXiv:1101.0811

58. Moore, C.J., Cole, R.H., Berry, C.P.: Gravitational-wave sensitivity curves. Classical and Quantum Gravity **32**(1), 015,014 (2015)

59. Mueller, G., McNamara, P., Thorpe, I., Camp, J.: Laser frequency stabilization for lisa (2005)

60. NASA Astrophysics Science Division: Astrogravs waveform catalogue. http://astrogravs.gsfc.nasa.gov/docs/catalog.html, [Accessed 30-August-2015] (2015)

61. Pacucci, F., Ferrara, A., Marassi, S.: Gravitational waves from direct collapse black holes formation. MNRAS **449**, 1076–1083 (2015). https://doi.org/10.1093/mnras/stv317. arXiv:1502.04125

62. Pain, I., Stobie, B., Wright, G.S., Paul, T., Cunningham, C.R.: Spire beam steering mirror: a cryogenic 2 axis mechanism for the herschel space observatory. In: Astronomical Telescopes and Instrumentation, International Society for Optics and Photonics, (pp. 619–627) (2003)

63. Paschotta, R.: Field Guide to Lasers, vol 12. SPIE press (2008)

64. Petrich, L.I., Shapiro, S.L., Wasserman, I.: Gravitational radiation from nonspherical infall into black holes. II - A catalog of 'exact' waveforms. ApJS **58**, 297–320 (1985). https://doi.org/10.1086/191043

65. Planck Collaboration, Ade, P.A.R., Aghanim, N., Armitage-Caplan, C., Arnaud, M., Ashdown, M., Atrio-Barandela, F., Aumont, J., Baccigalupi, C., Banday, A.J., et al.: Planck 2013 results. XVI. Cosmological Parameters **571**, A16 (2014). https://doi.org/10.1051/0004-6361/201321591. arXiv:1303.5076

66. Ricotti, M., Park, K.: Feedback-regulated accretion onto the first black holes. Am. Inst. Phys. Conf. Ser. **1480**, 297–302 (2012). https://doi.org/10.1063/1.4754371

67. Sabin, C., Bruschi, D.E., Ahmadi, M., Fuentes, I.: Phonon creation by gravitational waves. New J. Phys. **16**(8), 085,003 (2014). http://stacks.iop.org/1367-2630/16/i=8/a=085003

68. Saijo, M.: Dynamic black holes through gravitational collapse: Analysis of the multipole moment of the curvatures on the horizon. PhRvD **83**(12), 124031 (2011). https://doi.org/10.1103/PhysRevD.83.124031, arXiv:1106.1922

69. Schilling, J.: Silverbird Astronautics. http://silverbirdastronautics.com/LVperform.html (2009)

70. Schneider, R., Ferrara, A., Ciardi, B., Ferrari, V., Matarrese, S.: Gravitational wave signals from the collapse of the first stars. MNRAS **317**, 385–390 (2000). https://doi.org/10.1046/j.1365-8711.2000.03596.x, arXiv:astro-ph/9909419

71. Schott, A.: Zerodurr extremely low expansion glass ceramic (2016)

72. Seitenzahl, I.R., Herzog, M., Ruiter, A.J., Marquardt, K., Ohlmann, S.T., Röpke, F.K.: Neutrino and gravitational wave signal of a delayed-detonation model of type Ia supernovae. prd **92**(12), 124013 (2015). https://doi.org/10.1103/PhysRevD.92.124013. arXiv:1511.02542

73. Sereno, M., Sesana, A., Bleuler, A., Jetzer, P., Volonteri, M., Begelman, M.C.: Strong lensing of gravitational waves as seen by LISA. Phys Rev Lett **105**, 251,101 (2010). https://doi.org/10.1103/PhysRevLett.105.251101, arXiv:1011.5238

74. Shaddock, D.A., Ware, B., Spero, R., Vallisneri, M.: Post-processed time-delay interferometry for LISA. http://arxiv.org/pdf/gr-qc/0406106.pdf (2008)

75. SXS Collaboration: SXS Gravitational Waveform Database. http://www.black-holes.org/waveforms/, [Accessed 30-August-2015] (2015)

76. Tajmar, M., Genovese, A., Steiger, W.: Indium field emission electric propulsion microthruster experimental characterization. J. Propuls. Power **20**(2), 211–218 (2004)
77. Tanaka, Y., Nandra, K., Fabian, A.C., Inoue, H., Otani, C., Dotani, T., Hayashida, K., Iwasawa, K., Kii, T., Kunieda, H., Makino, F., Matsuoka, M.: Gravitationally redshifted emission implying an accretion disk and massive black hole in the active galaxy mcg-6-30-15. Nature **375**(6533), 659–661 (1995). https://doi.org/10.1038/375659a0
78. Tinto, M., Dhurandhar, S.V.: Time-delay interferometry. Living Reviews in Relativity **8**(4), 12–16 (2005)
79. Tyson, J.A.: Large synoptic survey telescope: overview. In: Astronomical Telescopes and Instrumentation, International Society for Optics and Photonics, (pp. 10–20) (2002)
80. Will, C.M.: Testing scalar - tensor gravity with gravitational wave observations of inspiraling compact binaries. Phys Rev D **50**, 6058–6067 (1994). https://doi.org/10.1103/PhysRevD.50.6058. arXiv:gr-qc/9406022
81. Wu, X.B., Wang, F., Fan, X., Yi, W., Zuo, W., Bian, F., Jiang, L., McGreer, I.D., Wang, R., Yang, J., Yang, Q., Thompson, D., Beletsky, Y.: An ultraluminous quasar with a twelve-billion-solar-mass black hole at redshift 6.30. Nature **518**, 512–515 (2015). https://doi.org/10.1038/nature14241. arXiv:1502.07418
82. Yagi, K.: Scientific Potential of Decigo Pathfinder and Testing GR with Space-Borne Gravitational Wave Interferometers. Int. J. Mod. Phys. D **22**, 1341013 (2013). https://doi.org/10.1142/S0218271813410137, arXiv:1302.2388
83. Yang, L., Lee, C.C., Geng, C.Q.: Gravitational waves in viable f(R) models. J. Cosmol. Astropart. Phys. **8**, 029 (2011). https://doi.org/10.1088/1475-7516/2011/08/029. arXiv:1106.5582
84. Yue, B., Ferrara, A., Salvaterra, R., Xu, Y., Chen, X.: The brief era of direct collapse black hole formation. MNRAS **440**, 1263–1273 (2014). https://doi.org/10.1093/mnras/stu351. arXiv:1402.5675
85. Zahnd, B., Zimmermann, M., Spörri, R.: Lisa-pathfinder cage and vent mechanism—development and qualification. In: Proceedings 15th European Space Mechanism and Tribology Symposium (ESMATS) (2013)